Institut de Physique Nucléaire de Lyon

Université Claude Bernard

IN2P3 - CNRS

LYCEN 2000/64
LPCC 00-010
August, 2000

Excitation energy and angular momentum of quasiprojectiles produced in the Xe + Sn collisions at incident energies between 25 and 50 MeV/nucleon

J-C. Steckmeyer, et al.
INDRA Collaboration

Submitted to Physical Review Letters

43, Boulevard du 11 Novembre 1918 - 69622 VILLEURBANNE Cedex - France

Excitation energy and angular momentum of quasiprojectiles produced in the Xe+Sn collisions at incident energies between 25 and 50 MeV/nucleon ⋆

J.C. Steckmeyer [a,1], E. Genouin-Duhamel [a], E. Vient [a], J. Colin [a], D. Durand [a], G. Auger [b], C.O. Bacri [c], N. Bellaize [a], B. Borderie [c], R. Bougault [a], B. Bouriquet [b], R. Brou [a], P. Buchet [d], J.L. Charvet [d], A. Chbihi [b], D. Cussol [a], R. Dayras [d], N. De Cesare [g], A. Demeyer [e], D. Doré [d], J.D. Frankland [b], E. Galichet [c,2], E. Gerlic [e], D. Guinet [e], S. Hudan [b], P. Lautesse [e], F. Lavaud [c], J.L. Laville [b], J.F. Lecolley [a], C. Leduc [e], R. Legrain [d], N. Le Neindre [a], O. Lopez [a], M. Louvel [a], A.M. Maskay [e], L. Nalpas [d], J. Normand [a], M. Pârlog [f], P. Pawłowski [c], E. Plagnol [c], M.F. Rivet [c], E. Rosato [g], F. Saint-Laurent [b,3], G. Tăbăcaru [f], B. Tamain [a], L. Tassan-Got [c], O. Tirel [b], K. Turzo [e], M. Vigilante [g], C. Volant [d] and J.P. Wieleczko. [b]

INDRA Collaboration

[a] *Laboratoire de Physique Corpusculaire, IN2P3-CNRS, ISMRA et Université, F-14050 Caen Cedex, France*

[b] *Grand Accélérateur National d'Ions Lourds, DSM-CEA/IN2P3-CNRS, BP 5027, F-14076 Caen Cedex 5, France*

[c] *Institut de Physique Nucléaire, IN2P3-CNRS, BP 1, F-91406 Orsay Cedex, France*

[d] *DAPNIA/SPhN, CEA/Saclay, Orme des Merisiers, F-91191 Gif-sur-Yvette Cedex, France*

[e] *Institut de Physique Nucléaire, IN2P3-CNRS et Université, F-69622 Villeurbanne Cedex, France*

[f] *National Institute for Physics and Nuclear Engineering, RO-76900 Bucharest-Măgurele, Romania*

[g] *Dipartimento di Scienze Fisiche e Sezione INFN, Università di Napoli "Federico II", I-80126 Napoli, Italy*

PACS: 25.70.-z, 25.70.Pq, 25.60.Pj

Abstract

The excitation energy and angular momentum transferred to quasiprojectiles have been measured in the $^{129}Xe+^{nat}Sn$ collisions at bombarding energies between 25 and 50 MeV/nucleon. The excitation energy of quasiprojectiles has been determined from the kinetic energy of all decay products (calorimetry). It increases with the violence of the collision, approaching 10 MeV/nucleon in the most dissipative ones. The angular momentum has been deduced from the kinetic energies and angular distributions of the emitted light charged particles (p, d, t, ^{3}He and α). The (apparent) spin value decreases with the violence of the collision. Larger spin values are observed at the lowest bombarding energy. Data are compared with the predictions of dynamical and statistical models. They reproduce the data in a quantitative way indicating that large spin values are transferred to quasiprojectiles during the interaction. The results show that the one-body dissipation formalism still applies at intermediate bombarding energies and low energy dissipations. With the increase of the energy, the data seem to be better described when the two-body interaction is accounted for.

⋆ experiment performed at Ganil

[1] E-mail: steck@in2p3.fr

[2] CNAM, Laboratoire des Sciences Nucléaires, F-75003 Paris, France

[3] Present address: DRFC/STEP CEA/Cadarache, F-13108 Saint-Paul-lez-Durance, France

1 Introduction

In the interaction between projectile and target nuclei, energy and angular momentum are dissipated into some degrees of freedom. A part of the kinetic energy is converted into intrinsic excitation energy of the quasiprojectile (QP) and quasitarget (QT) nuclei. This energy is then exhausted in various decay modes [1,2]: (i) sequential emission of γ rays, neutrons and/or light charged particles (LCP's), (ii) fission of the nucleus in two fragments and (iii) simultaneous and/or prompt breakup in many fragments (the so-called multifragmentation process). Accordingly, the knowledge of the excitation energy is a key quantity to investigate any process.

The initial orbital angular momentum is shared between relative motion and intrinsic spins to QP and QT nuclei. At incident energies smaller than 10 MeV/nucleon, the angular momentum transfer (AMT) was studied measuring the decay products of the nuclei: multiplicity and angular distributions of γ rays [3,4] angular distributions of LCP's [5] or fission fragments in case of a heavy nucleus [6–8]. Large spin values are transferred to the nuclei during the interaction (several tenths of $\hbar$ units) and AMT is strongly aligned along the normal to the reaction plane [9]. Statistical [10] as well as transport [11] models are equally successful in the description of the data.

At incident energies higher than 100 MeV/nucleon the participant-spectator model predicts two remnants and a fireball which do not or weakly interact between each other. Therefore no correlation is expected between AMT and the spectators. One measurement performed at several hundreds of MeV/nucleon indicates that the QP is left at the end of the interaction without spin, suggesting that reaction mechanisms different from those observed at low energy could prevail at these energies [12].

At intermediate incident energies ($10 < E_{bomb} < 100$ MeV/nucleon) only few results are available [13–15]. Their interpretation is more complex than in the low energy case as this transition regime is dealing with excited nuclei emitting many particles. Studying AMT in this energy domain can provide information for a better understanding of the following points: (i) the real nature of the underlying reaction mechanisms of AMT (exchange of nucleons [11], excitation of collective modes [10,16,17]), (ii) the equilibration time for the dissipation of the angular momentum in heavy ion collisions [18], (iii) the viscosity of the nuclear matter (tangential friction forces) [19] and (iv) the influence of angular momentum on the deexcitation of hot nuclei [20].

This paper reports on the determination of the excitation energy and angular momentum transferred to QP's in the ^{129}Xe+^{nat}Sn collisions at 25, 39 and 50 MeV/nucleon. The aim of this study is to extract key quantities from the experimental data as carefully as possible. These quantities may help to constrain the predictions of theoretical models. Along this article, experimental data and theoretical predictions will be shown as a function of the violence of the collision. For this purpose the transverse energy of LCP's and the charge of the detected QP residue will be used alternatively as a rough estimate of the dissipation.

The paper is organized as follows. Sect. 2 briefly describes the experimental conditions. In

sect. 3 are detailed the different procedures used to reconstruct the characteristics of QP's. The results on the excitation energy are given in sect. 4. The spin values extracted from the kinetic energy spectra of LCP's are shown in sect. 5. Sect. 6 is devoted to the construction of angular distributions of LCP's in the QP frame. They are compared with simulated distributions in sect. 7. The spin characteristics are extracted in sect. 8. The evolution of the spin as a function of the charge of the QP residue and the bombarding energy is studied in sect. 9. Results and discussions are presented in sect. 10 and conclusions are drawn in sect. 11.

2 Experimental conditions

The experiment was performed at the Ganil accelerator using the Indra detector [21]. Let us recall that the detector is composed of 17 rings centered on the beam axis. Depending upon the polar angle, detection modules have two or three detector layers: NE102 and NE115 plastic scintillators ($2° < \Theta \leq 3°$) [22], ionization chamber, silicon detector and CsI(Tl) scintillator ($3° < \Theta \leq 45°$) and ionization chamber and CsI(Tl) scintillator ($45° < \Theta \leq 88°$ and $92° < \Theta \leq 176°$). The overall geometrical efficiency is 90% of 4π. Isotopic identification is achieved for $Z \leq 4$ particles. At angles smaller than 45° fragments are identified in atomic number up to and better than Z=54. Beyond 45° the identification is achieved up to $Z \approx 20$ with a resolution of one charge unit. More about the performances of Indra as well as on the calibration procedures can be found in refs. [21,22].

A thin target of natural Sn (350 μg.cm^{-2}) was bombarded by ^{129}Xe projectiles at incident energies of 25, 39 and 50 MeV/nucleon. Events were registered when at least four detectors fired. Low intensity beams were used to keep random coincidences at a very low level (below 10^{-4}).

3 Reconstruction of the quasiprojectile

3.1 Description of the data

One of the most striking features emerging from collisions between heavy ions at intermediate bombarding energies is the binary character of these collisions: two main fragments emerge in the exit channel after the interaction. The charges, masses and velocities of these fragments are close to that of the projectile and target in peripheral collisions, and move away more and more as the energy dissipation increases. The binary character has been recognized in light systems [23–26], in medium mass systems [27,28] as well as in heavy ones [29–31], measuring the characteristics of LCP's and fragments.

The ^{129}Xe+^{nat}Sn collisions measured at incident energies between 25 and 50 MeV/nucleon show the same trends [32–35]. When plotting the invariant cross-section $\frac{d^2\sigma}{V_\perp dV_\parallel dV_\perp}$ of LCP's

in the velocity plane, two sources come out, well separated from each other at the highest incident energy and for large impact parameters. The relative velocity between the two heavy partners decreases with the decrease of the incident energy and with the increase of the violence of the collision. By only looking at invariant cross-section in the velocity plane, it is no longer possible, for the lowest impact parameters, to distinguish between the two following scenarios: two sources very close from each other or one single source (for example see fig. 2 of ref. [33]).

However, unlike to what is observed at low bombarding energies ($<$ 10 MeV/nucleon), deviations with respect to a binary scenario are observed: particles are abundantly produced with velocities between the projectile and target velocities. Such a behaviour appears for both LCP's and intermediate mass fragments (IMF's) [33]. This mid-velocity contribution is usually attributed to a preequilibrium emission [36] or to a neck emission (the two outgoing partners being bound each other with a neck of nuclear matter) [37,38]. These non statistical emissions are studied in specific papers [33,34,39] and will not be considered in this work. On the contrary, we will try to avoid these particles to only deal with particles isotropically emitted from QP, which is then assumed to be equilibrated in shape.

As already stated we are interested in studying the characteristics of QP's produced in the ^{129}Xe+^{nat}Sn collisions. QP's are produced in collisions ranging from the more peripheral ones to very central ones, with a large range in the damping of the relative motion. Therefore, measuring QP's in these collisions offers the possibility for studying the formation and deexcitation properties of nuclei on a large range of excitation energy.

Several methods have been proposed in the past to reconstruct the characteristics of QP's (charge, mass and excitation energy) [40–44]. They all suffer from the same drawbacks. There is no possibility to separate unambiguously particles sequentially emitted by QP's and particles originating in other processes such as direct reactions, preequilibrium emission or emission from a neck of nuclear matter located between the projectile and target. Indeed the sequential and non sequential particles are emitted with time scales not very different from one process to the other one. Furthermore there is no reason to believe that the different processes occur in a well defined time sequence: there is no sharp cutoff in time, the processes overlap. Another serious drawback is that the hierarchy of the emission times of the particles is unknown. How to reconstruct the nucleus while the sequence of its desintegration has been missed by the experiment? As an example, the recoil effects can be important in case of light or medium mass nuclei [45]. Finally the experimental setup introduces biases which have to be perfectly understood to interpret the data in a right way [46].

Instead of searching for a new miracle method, we will use several tested procedures and compare their results to deduce general trends as for the characteristics of QP's. It will be shown that sizeable uncertainties are associated with the absolute values of the charge, mass and excitation energy of QP's. On the other hand all these procedures agree qualitatively when looking at the excitation energy per nucleon.

For the purpose of the analysis, we selected "complete events" in which more than 80% of the total charge and of the incident linear momentum have been detected by the experimental setup. Another event selection will be performed when studying the angular momentum

transfer (see sect. 5 and following).

3.2 Description of the reconstruction procedures

All the procedures are based on the determination of the source velocity (or QP velocity). Once the source velocity is known, the charge is calculated by adding up the charges of all particles and fragments belonging to the source. At this step we assume that all particles emitted in the forward hemisphere in the frame of the source are evaporated by this source. This strong assumption relies on the fact that the angular distributions of particles are isotropic in the forward hemisphere of the source. This is also the reason why we talk about equilibrated nuclei [24,26].

The mass is deduced from the charge assuming the same A/Z ratio as that of the projectile. Finally the excitation energy is obtained from the kinetic energies of all products (calorimetry method). The kinetic energy of neutrons, not detected in the experiment, is estimated.

3.2.1 Method I

The V_{QP} velocity is calculated from the weighted velocities of all IMF's ($Z \geq 3$) detected with a velocity larger than or equal to the velocity of the center of mass of the reaction (V_{cm}). This limit has been chosen as we are dealing with an almost symmetrical system. To reconstruct the total charge of the QP, only LCP's and IMF's emitted in the forward hemisphere in the QP frame are taken into account. They are added up to the charge of the QP residue (Z_{max}), their number being doubled to simulate the contribution of the backward emitted particles:

$$Z_{QP} = Z_{max} + 2 \sum_{i=1}^{M_{LCP}+M_{IMF}} Z_i \qquad (1)$$

This artefact has been chosen to avoid to integrate LCP's and IMF's emitted with velocities intermediate between the velocities of the projectile and target. In eq. (1), M_{LCP} and M_{IMF} are the multiplicities of LCP's and IMF's emitted in the forward hemisphere of the QP, respectively.

IMF's backward emitted in the QP frame are accounted for in the reconstruction of the source velocity and not in that of the total charge. Although this could be appear as an inconsistency, it will allow to test the influence of IMF's on the QP charge determination when comparing the results of this method with those of method IV.

The excitation energy is then determined by the calorimetry method from the following equation:

$$E^* = -Q + 2 \sum_{i=1}^{M_{LCP}+M_{IMF}} K_i + \sum_{j=1}^{M_n} K_j + K_{Z_{max}} \qquad (2)$$

where K_i and K_j are the kinetic energies of the i^{th} charged particle and of the j^{th} neutron, respectively. Q is the Q-value of the reaction. The neutron multiplicity is obtained from mass

conservation:

$$M_n = Z_{QP} \times (A/Z)_{PROJ} - 2 \sum_{i=1}^{M_{LCP}+M_{IMF}} A_i - A_{Z_{max}} \quad (3)$$

For the kinetic energy of the neutrons, we used either the kinetic energy of the protons minus the Coulomb barrier or we assumed a mean kinetic energy equal to $2 \times T$, T being linked to the excitation energy by the Fermi gas relationship: $E^* = a \times T^2$ [48]. In that case the temperature T is deduced by solving eq. (2) in which E^* is replaced by its value $a \times T^2$.

LCP's have been found to be emitted preferentially in the early steps of the deexcitation cascade [47]. Taking for the neutron kinetic energy the value of $1.5 \times T$, instead of $2 \times T$, would decrease the excitation energy by 9% and using A/10 instead of A/8 for the level density parameter would lead to a decrease of 6%.

3.2.2 Method II

The QP velocity is taken equal to the velocity of the biggest fragment ($V_{Z_{max}}$) detected in the forward hemisphere in the c.m. of the reaction [43]. This fragment is assumed to be the QP residue. Taking $V_{Z_{max}}$ as the source velocity explicitely assumes that the source velocity is not perturbed by the successive emissions of IMF's and LCP's all along the deexcitation chain. To calculate the QP charge as well as its excitation energy we take into account (i) all particles emitted in the forward hemisphere of the frame of the biggest fragment and (ii) all IMF's and LCP's emitted in the backward hemisphere with relative velocities smaller than a given velocity. From the comparison of the velocity distributions of LCP's and IMF's emitted at forward and backward angles in the frame of the biggest fragment, the following velocity cut values have been retained: 3.5, 5. and 6. cm/ns for IMF's ($Z \geq 3$), Z=2 and Z=1, respectively [48].

The charge, excitation energy and neutron multiplicity of the QP are calculated using eqs. (1-3) in which the second term of each right hand side member has no longer the factor 2 in front of it as $M_{LCP} + M_{IMF}$ is now the total multiplicity of LCP's and IMF's emitted by the QP in the whole space.

3.2.3 Method III

We use the thrust variable [32,49] defined as:

$$T_2 = \frac{|\sum_{i \in S_1} \vec{P}_i| + |\sum_{j \in S_2} \vec{P}_j|}{\sum_{k=1}^{M_{IMF}} |\vec{P}_k|} \quad (4)$$

In case of a strictly binary configuration involving two nuclei S_1 and S_2 the value of the thrust variable is equal to 1. This is the case for the elastic scattering for example. The maximisation of the thrust variable allows for the construction of two ensembles of IMF's which are then associated with the QP and QT. Only IMF's are considered to avoid including LCP's emitted at mid-velocities which otherwise will reduce artificially the relative velocity between the two sources. Such a method has been applied successfully to the source determination in case of

almost symmetrical systems. The source velocities so deduced are coherent with the velocities inferred from the behaviour of LCP's [32,33,35].

In the case of quasi symmetrical systems, the dissipated energy per nucleon can be simply expressed as a function of the available c.m. kinetic energy per nucleon ϵ_{cm} and of the relative velocity between the two sources V_{rel} [32,35]:

$$\epsilon_{diss} = \epsilon_{cm} - V_{rel}^2/8 \tag{5}$$

To compare the results of this method with those of the other methods, the excitation energy per nucleon of the QP will be assumed equal to the quantity ϵ_{diss} [32,35].

3.2.4 Method III+I

The last method is the result of a combination of the methods I and III. The source velocity is calculated from the weighted velocities of all IMF's which constitute the QP, the set of IMF's being reconstructed with the help of the thrust variable described above. Then the QP charge is obtained by summing all IMF's belonging to the QP set and twice all LCP's emitted in the forward hemisphere in the QP frame.

No strong difference between this method and the first one is expected as the IMF selections are identical for the source velocity determination. The only difference lies on the influence of IMF's on the QP charge: they are counted twice (in the QP forward hemisphere) in method I while they are counted only once in this method.

4 Excitation energy of QP's: results and discussion

The excitation energy per nucleon of QP's calculated according to the methods described above is shown in fig. 1 as a function of the transverse energy of Z=1 and 2 particles, together with the source velocity and the total charge of the source. The transverse energy is calculated for each event from the linear momentum component perpendicular to the beam axis and used as a sorting parameter to appraise the violence of the collision. These results concern the ^{129}Xe+^{nat}Sn collisions at 50 MeV/nucleon of bombarding energy. Only complete events, for which more than 80% of the total charge and total momentum were collected, have been kept for the sake of comparison.

There is no big difference on the parallel component of the source velocity in the c.m. system (cf. fig. 1-a). Method II leads to slightly higher values than methods I and III which are basically the same, both including IMF's which contribute to decrease the source velocity as they exhibit a slight excess in the backward hemisphere of the QP residue.

The total charge of the source, displayed in fig. 1-b, shows practically no evolution with the violence of the collision except for the smallest transverse energies. According to the different methods the Z_{QP} charge varies between $\approx$ 40 and 45 charge units which corresponds to a

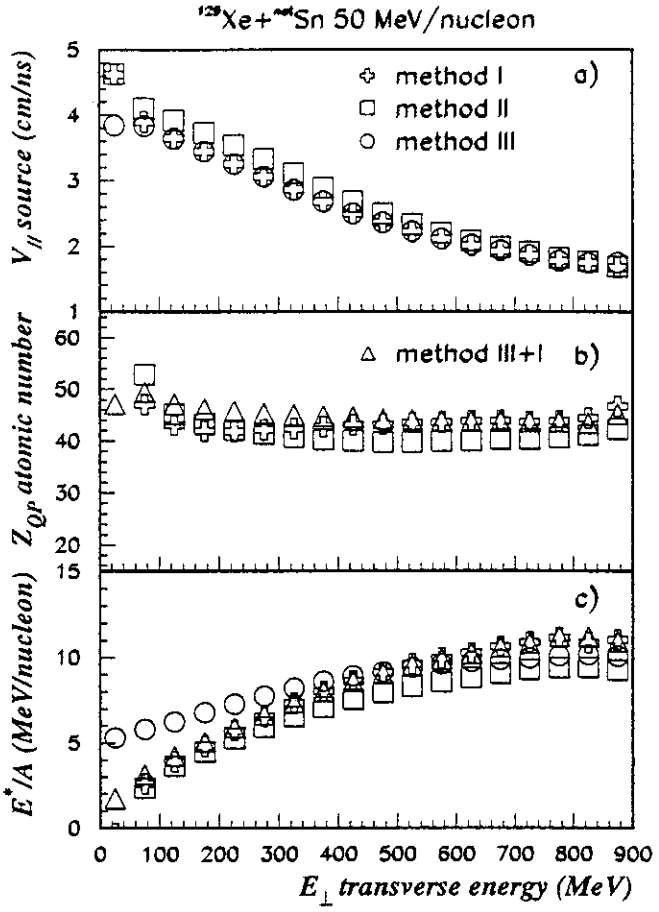

Fig. 1. Comparaison of the different methods (see text) used to determine the c.m. parallel velocity component (-a), total charge (-b) and excitation energy per nucleon (-c) of QP's in the ^{129}Xe+^{nat}Sn collisions at 50 MeV/nucleon.

deficit in charge of 15-25% of the projectile charge. This fraction could be associated with the nucleons lost by the projectile in non statistical emissions, the loss of particles due to the experimental setup being of second order.

The excitation energy increases with the increase of the transverse energy, i-e with the violence of the collision. For the smallest $E_\perp$ values the excitation energy is less than 2 MeV/nucleon. Recall that we are dealing with complete events: this selection requires a minimum energy dissipation to collect sufficient information, in particular for QT's products which have to overcome detection thresholds. Then the excitation energy increases linearly with $E_\perp$ up to a value of 500-600 MeV, and seems to saturate, whatever the method used, at a value between 9 and 11 MeV/nucleon.

By looking at the results in more details, we observe practically no difference between methods I and I+III as expected (see subsect. 3.2.4), except slightly smaller Z_{QP} values with method I for low transverse energies. Method II leads systematically to lower values. This is due to the selection: less LCP's and IMF's are accounted for in the QP frame, the source velocity being slightly larger than the one obtained with method I. As a result the charge

and mass of QP's are smaller, their total excitation energy is smaller, but due to the smaller masses, a compensation effect occurs and the excitation energy per nucleon differs only by $\approx$ 20% with respect to the results of method I.

Clearly different are the results of the method III, particularly for the smallest $E_\perp$ values. The technique based on the thrust variable needs the event be detected as completely as possible. Due to the detection thresholds most of the events associated with large impact parameters are badly detected: the target and its decay products have too low velocities. Consequently, the velocity of the reconstructed QT, in the laboratory system, is larger than it should be, and the relative velocity smaller. From eq. (5), it is seen that a too small relative velocity results in a too high dissipated energy.

As stated in the previous section, the aim of this study is not to find the best method to reconstruct and determine the excitation energy of QP's. Each method has its advantages and drawbacks. The main interest is to evaluate the uncertainty on the reconstruction of QP's. In fig. 1-c it is seen that all methods agree within $\pm$ 10%, except method III at low $E_\perp$ values. This comparison gives some confidence in the results displayed in fig. 1-c. Therefore it can be stated that QP's are produced with high excitation energies approaching (10 $\pm$ 1) MeV/nucleon in the most violent collisions.

We have to recall that these results rely on some hypotheses: all particles emitted in the forward hemisphere of the source are evaporated by the source and there is a forward-backward symmetry.

Semi-classical calculations have been undertaken to study the mid-velocity particles in the light system ^{36}Ar+^{27}Al [50]. It is shown in this work that fast particles can be observed in the forward hemisphere of the source and that their angular distribution can be isotropic alike the distribution of the particles sequentially emitted by the source. In this framework the excitation energy is thought to be smaller than the one derived from the experiment [24]. In a recent work [51], an attempt has been done to estimate the excitation energy of QP's removing all mid-velocity particles which are found to populate the whole range of parallel velocities [39]. So the excitation energy of QP's produced in the ^{36}Ar+^{58}Ni system at 95 MeV/nucleon is shown to be strongly reduced with respect to a binary picture which assumes no preequilibrium and then leads to the largest possible excitation energy.

What about the ^{129}Xe+^{nat}Sn collisions? The yield of mid-velocity particles seems to be smaller in the ^{129}Xe+^{nat}Sn system than in the lighter system ^{36}Ar+^{58}Ni: at intermediate impact parameters, the mid-velocity contribution is 20% of the total charge of projectile in the former one [33] not very far from the rough estimation deduced from Z_{QP} (see above and fig. 1-b), while it is 30% in the latter one [39]. Neglecting Z=1 particles which constitute the larger fraction ($\approx$ 60%) of the mid-velocity contribution leads to a reduction of the QP excitation energy per nucleon of 20-25% in the case of the ^{129}Xe+^{nat}Sn at 50 MeV/nucleon. Consequently it is believed that the values shown in fig. 1-c are reasonable estimates of the excitation energy of QP's, although likely picturing upper limits of the excitation energy.

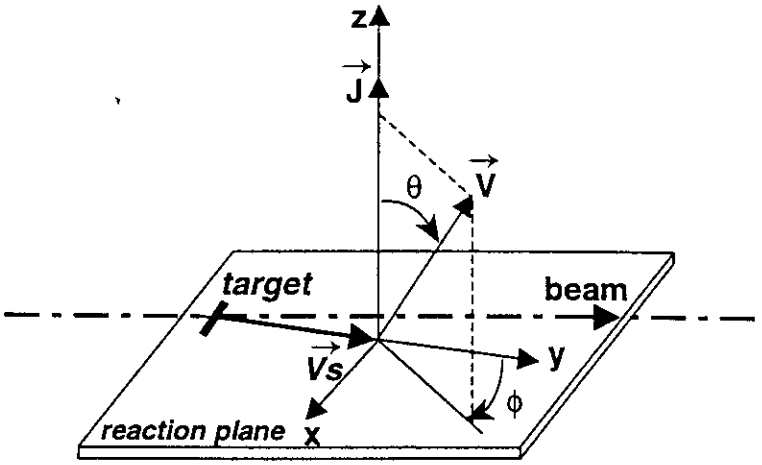

Fig. 2. Rest frame of the emitter. Θ and Φ are the out-of-plane and in-plane emission angles of the particle. The reaction plane is defined by the beam direction and the velocity vector of the source V_S (V_S is aligned on the Y-axis). The spin is aligned along the normal to the reaction plane (Z-axis). $\Phi > 0°$ corresponds to positive velocity components on the X-axis.

5 Spin values of QP's extracted from the kinetic energy spectra of LCP's

A decaying nucleus in rotation will mainly emit particles in a plane perpendicular to the spin axis. The extra kinetic energy imparted to the particles is maximum when the direction of emission is perpendicular to the spin and zero when the emission occurs along the spin axis. In principle, from the difference between the mean kinetic energies of particles emitted along these two directions, it should be possible to extract the spin value of the nucleus. Indeed the average kinetic energy of a particle emitted by a spherical nucleus in rotation [52] is given by the following relation:

$$< E(\Theta) > \approx B + 2T + T\ \sin^2(\Theta)/2\sigma^2 \tag{6}$$

where the two first terms of the right hand side are the Coulomb barrier for the emission of the particle and the contribution from the thermal energy. The third term is an extra energy driven by the angular momentum. It is maximum in the reaction plane at $\Theta = 90°$ (cf. fig. 2). The reaction plane is defined by the velocity vectors of the beam and of the source.

The σ parameter can be expressed as:

$$\sigma^2 = \frac{IT}{\hbar^2 J^2} \times \frac{I + \mu R^2}{\mu R^2} \tag{7}$$

where J is the spin of the emitter, I and T the moment of inertia and the temperature of the residual nucleus and μR^2 the relative moment of inertia of the configuration composed from the daughter nucleus and the light ejectile. Eq. (7) has been derived assuming $\mu R^2 \ll I$.

The difference $\Delta <$ E $>$ between the energies measured at $\Theta = 90°$ and $0°$ allows for the

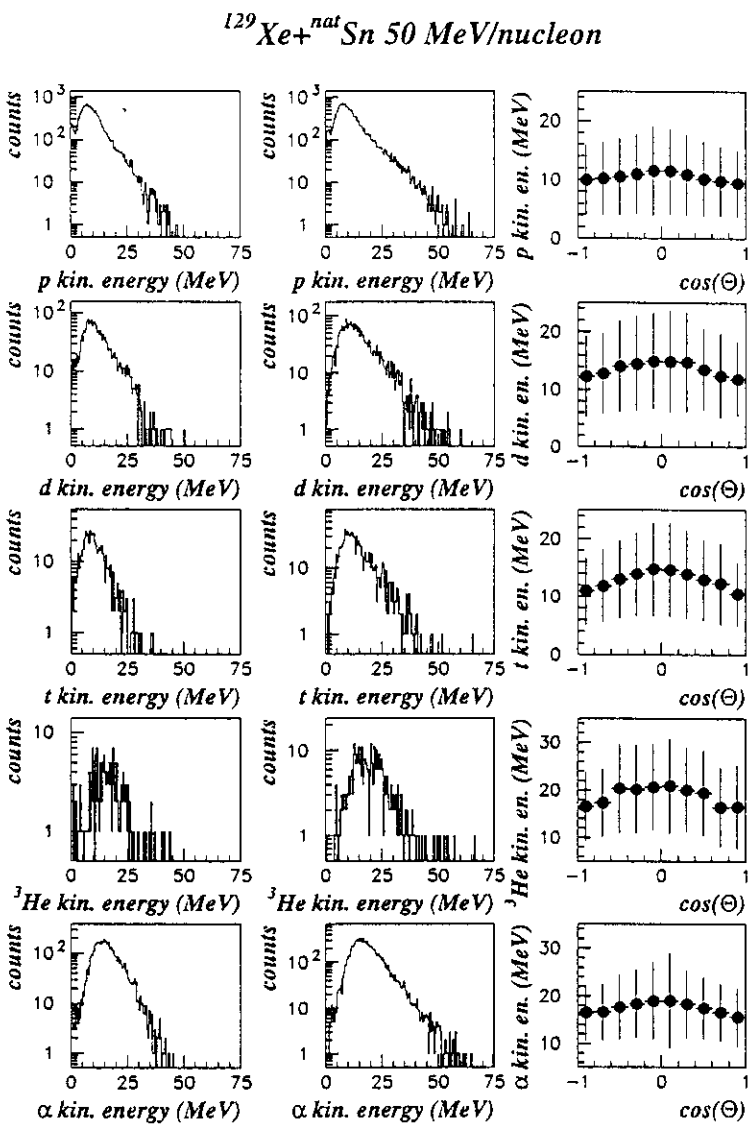

Fig. 3. Kinetic energy spectra of LCP's measured along the normal to the reaction plane (left column) and in the reaction plane (middle column). Mean values of the kinetic energy spectra as a function of the Θ out-of-plane angle (right column). These data are associated with $50 < E_{\perp} \leq 100$ MeV. All spectra and associated mean values are built in the QP frame. Uncertainties on the mean energy determination are shown as error bars (right column).

determination of the spin of the nucleus according to the following relation:

$$J \approx \frac{I}{\hbar} \sqrt{\frac{2\,\Delta < E >}{\mu R^2}} \tag{8}$$

According to this method the estimation of the spin is independent of the temperature of the residual nucleus (cf. sect. 8).

In this section and the following ones, all events detected with more than 70% of the incident momentum are considered: it has been shown that they are associated with a complete detection of the QP and its deexcitation products [48].

To determine the spin value of QP's we need to construct the kinetic energy spectra of LCP's in the frame of the source. The source characteristics are deduced with the help of method I (cf. subsect. 3.2.1). The emission angles of LCP's (Θ and Φ, cf. fig. 2) are calculated and the energy spectra are built. They are shown in fig. 3 for different types of LCP's: protons, deuterons, tritons, ^{3}He and α particles. The left column in fig. 3 displays the kinetic energy spectra of LCP's emitted along the normal to the reaction plane ($|\cos(\Theta)| > .8$), while the column in the middle shows the kinetic energy spectra of LCP's emitted in the reaction plane ($|\cos(\Theta)| < .2$). These spectra are integrated over the angular range $-90° \leq \Phi \leq 90°$. The right column in fig. 3 displays the variation of the mean kinetic energy as a function of the cosine of the Θ out-of-plane angle. As expected the mean kinetic energies exhibit a maximum in the reaction plane ($\cos\Theta = 0$).

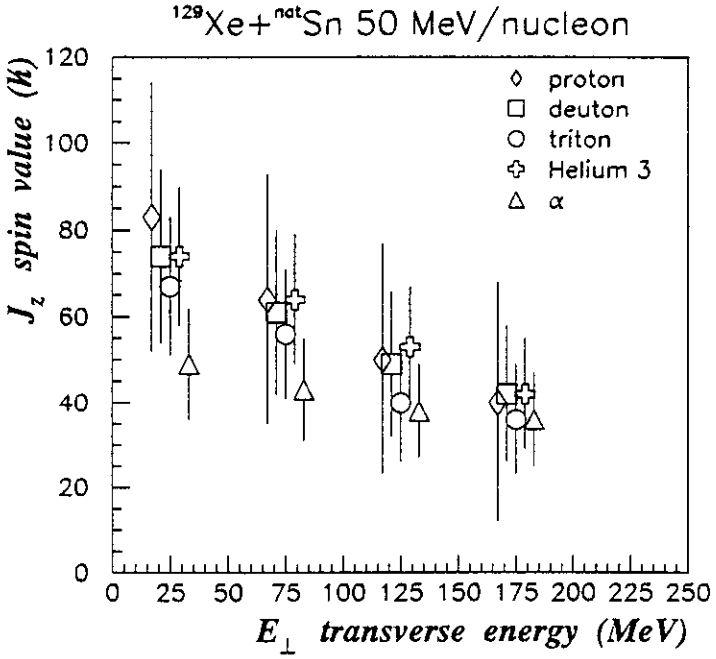

Fig. 4. Spin values of QP's deduced from the mean values of the kinetic energy spectra of LCP's as a function of the transverse energy (see text). For clarity, symbols have been shifted along the abscissa axis. Uncertainties on the spin determination are shown as error bars.

The $\Delta < E >$ values are derived from the data with a fitting procedure. Spin values are then deduced for all particles and for different $E_\perp$ bins. All results are given in fig. 4. As seen, rather large uncertainties affect the experimental values. Besides the error on the determination of the σ value, they are due to the assumptions made on the mass of QP's and on the radius parameter used in the calculations of the moments of inertia ($r_\circ = 1.22$ fm) [48]. In fig. 4 the spin values decrease with the increase of the transverse energy. We would expect the opposite behaviour, i-e an increase of the spin as a function of the transverse energy: in peripheral heavy ion reactions, the angular momentum transferred to the nuclei grows up with the number of exchanged nucleons, and therefore with the increase of the dissipation (see later in sect. 8).

6 Experimental angular distributions of LCP's

As written in the introduction, the angular distributions of LCP's reflect the spin characteristics of the emitter. In principle it should be possible to access the whole spin distribution: the aligned part as well as the dealigned components [10,11]. Assuming no dealignment of the spin, the angular distribution of emitted LCP's in the rest frame of the emitter is given by the following relation:

$$W(\Theta) \approx \exp(-\cos^2(\Theta)/2\sigma^2) \tag{9}$$

where Θ is the out-of-plane angle with respect to the spin axis (see fig. 2). The expression of the width σ is given in eq. (7).

The angular distribution W(Θ) is anisotropic with a maximum at $\Theta = 90°$ in the reaction plane. The anisotropy increases with the increase of the spin of the emitter and with the increase of the particle mass, it decreases with the increase of the temperature. From the width σ of the angular distribution the spin of the nucleus can be extracted, provided that T is known (see eq. (7)).

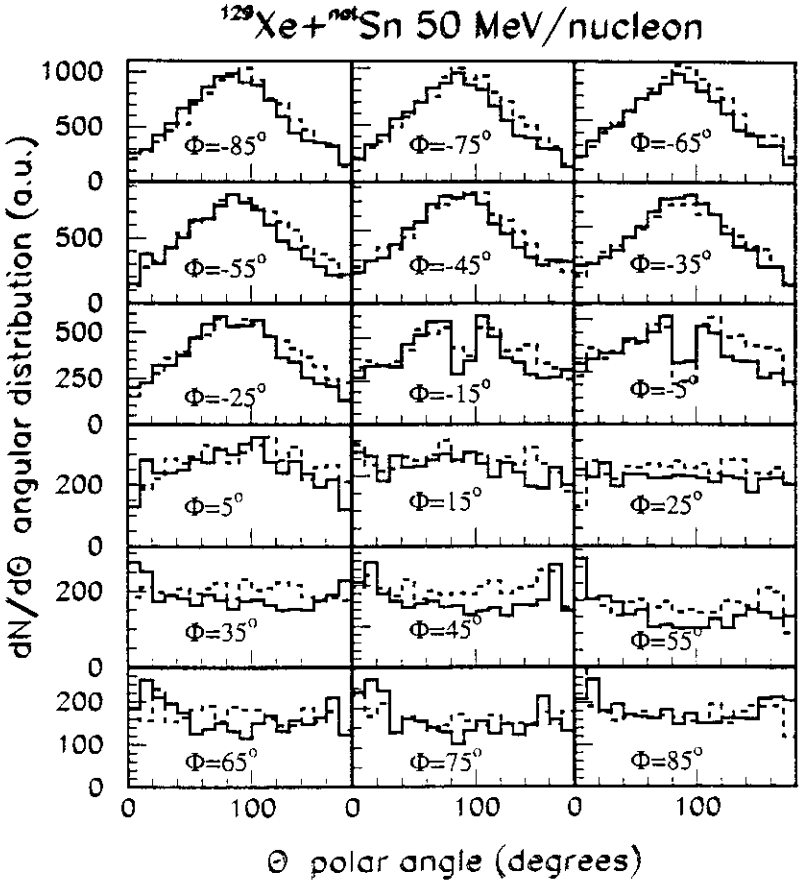

Fig. 5. Out-of-plane angular distributions shown as a function of the in-plane angle. These data concern α particles emitted from QP's produced in events with $50 < E_\perp \leq 100$ MeV. Solid lines are the data, dashed lines are results of a simulation.

Method I has been used to reconstruct the characteristics of QP's (cf. subsect. 3.2.1). It has been intensively checked [48] with the help of simulations performed with the Simon code [53]. Once the source velocity is known, the Θ and Φ angles are calculated and the angular distribution built. Solid lines in fig. 5 show as a function of the Φ in-plane angle, the out-of-plane angular distributions of α particles emitted by QP's produced in events having a $E_\perp$ transverse energy between 50 and 100 MeV. Anisotropic angular distributions with a maximum at $\Theta = 90°$ are observed at negative in-plane angles while flat distributions are observed at positive in-plane angles. Such a behaviour is unexpected as an anisotropic shape should be observed for positive in-plane angles too. The shape of the angular distribution shows an excess of particles on the other side of the beam with respect to the direction of the detected QP residue (see fig. 6-b). In this figure is shown in the laboratory frame the invariant cross section of α particles associated to QP's produced with $150 < E_\perp \leq 200$ MeV. The excess of particles develops for negative $V_\perp$ transverse velocities on the opposite side of QP's which fly with positive transverse velocities. Fig. 6-b points out two effects: in the QP forward hemisphere (for $V_\parallel > 9$ cm/ns) more α particles are measured at negative transverse velocities than at positive ones. This effect, which will be explained and simulated in the following paragraphs, has nothing to do with the second one: the excess of α particles always located at negative transverse velocities in the QP backward hemisphere with $V_\parallel \approx 7$ cm/ns (rectangular zone in fig. 6-b). These particles are attributed to the mid-velocity contribution and strongly remind the non equilibrium emission process observed in refs. [28,54]. Their role will be discussed in sect. 9.

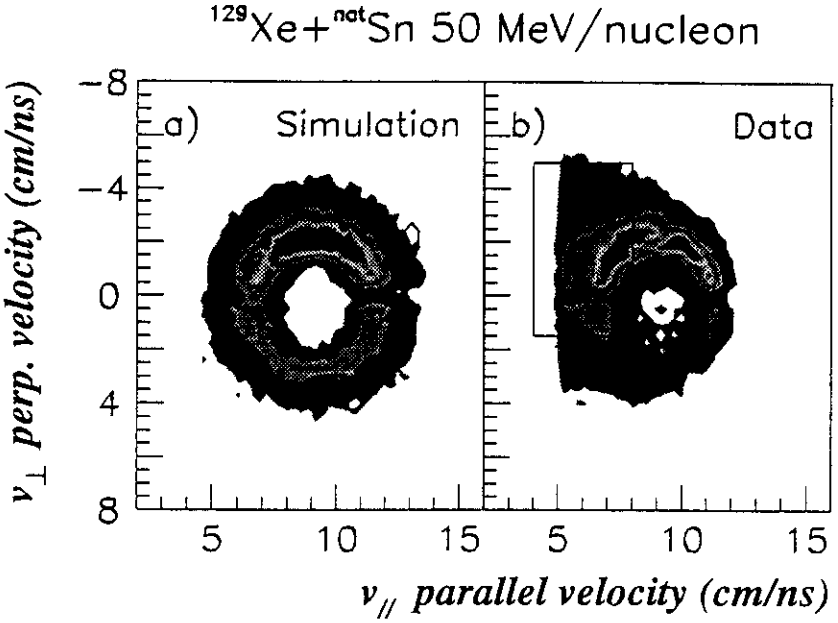

Fig. 6. Invariant cross section of α particles associated to QP's produced in events with $150 < E_\perp \leq 200$ MeV (see text): simulation in a) and experimental data in b). The QP velocity components are $V_\parallel$=9.0 cm/ns and $V_\perp$=.3 cm/ns.

An anisotropy of particles in the QP forward hemisphere is also observed with hydrogen isotopes and ^{3}He nuclei. This imbalance increases with the mass of the isotope: the heavier the mass is, the further away from QP it is pushed. This suggests an effect linked to momentum

conservation. As a matter of fact, it is well known that the angular distributions of QP's are very forward peaked at intermediate bombarding energies [55,56]. With the increase of the energy the forward focusing is expected to be stronger. As a consequence, for a given detector angle of the QP residue, configurations where primary QP's have been emitted at smaller angles are much more favoured than configurations where QP's have been emitted at larger angles. If QP's were produced according to an isotropic angular distribution we should observe isotropic in-plane angular distributions for the emitted particles, leading to identical out-of-plane angular distributions whatever the in-plane angle. This has been checked with simulations.

Due to the strong evolution of the angular distribution of QP's, the spin values can no longer be simply accessed from the width of the out-of-plane distributions of LCP's. They have to be unfolded from the angular distributions of QP's. The proper way to extract the spin value from the data would be to perform theoretical calculations filtered by the experimental setup and reproducing at the same time all observables: charge, energy, multiplicity and angular distributions of all charged products. These calculations should describe the mid-velocity component too. Furthermore, in order to fit the whole experimental data with the results of the calculations, a lot of simulations, with different sets of input values would have to be done. Currently such a procedure is unthinkable. Instead a simple simulation has been developed.

7 Simulation of the angular distributions of LCP's

The ingredients of the simulation are the following ones. The QP is produced with given charge, velocity and angular distributions. It emits only one type of particle with energy and multiplicity distributions taken from the experiment. This hypothesis can appear as an oversimplification. Actually it can be considered as a substitute for simulating the whole deexcitation chain since we use experimental distributions which, de facto, includes all time sequence effects in the deexcitation. The simulated events are filtered by the experimental setup. We use a simple geometrical filter as the perturbation introduced by the apparatus is weak, due (i) to the good detection performances of Indra for the fast charged products and (ii) to the low or moderate multiplicities associated to the events under consideration. The calculations are done by varying the charge, velocity and angular distributions of the QP, till the charge, velocity and angular distributions of the simulated residue reproduce the corresponding experimental distributions.

Once the calculation reproduces the characteristics of the detected residue, the initial charge, velocity and angular distributions of the QP are kept and used as a starting point for new calculations in which the value of the σ parameter (eq. (7)) is then varied on a large domain. The value which is retained at the end of the procedure is the one which minimizes the difference between the simulated and experimental angular distributions of LCP's [48].

In fig. 7 are displayed results of simulations for QP's produced in collisions of ^{129}Xe+^{nat}Sn at 50 MeV/nucleon of bombarding energy. These events are associated with moderate transverse

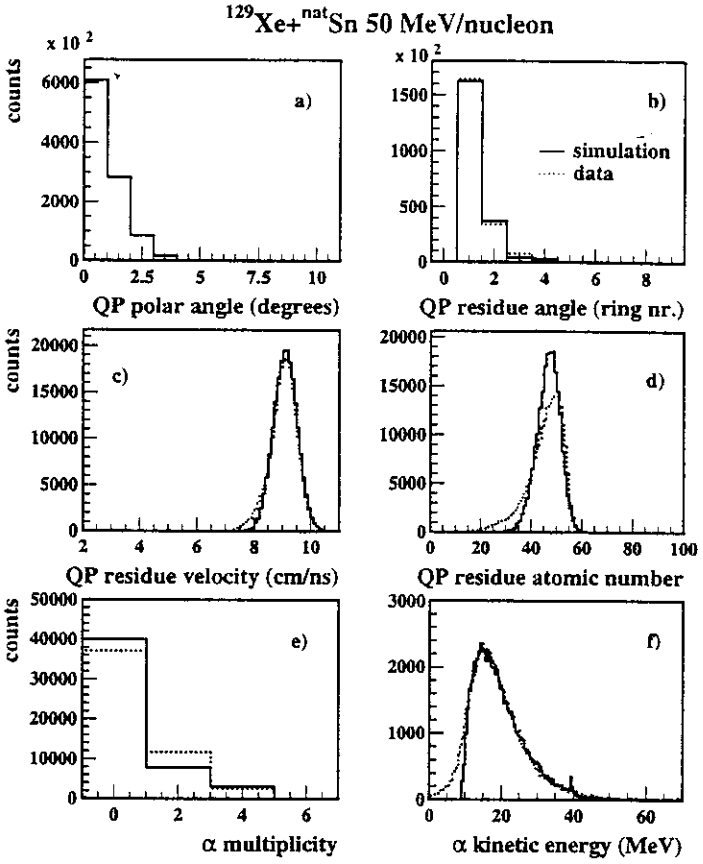

Fig. 7. Angular distribution of primary QP's (-a) and of QP residues (-b). Parallel velocity (-c) and atomic number (-d) distributions of QP residues. Multiplicity (-e) and kinetic energy (-e) distributions of α particles emitted by QP's. The data refer to events associated with $50 < E_\perp \leq 100$ MeV.

energies ($50 < E_\perp \leq 100$ MeV) and only deal with α particles. The angular distribution of QP's is shown in fig. 7-a sampled on an exponential distribution $\exp(-k\Theta_{pol})$ [55,56]. The angular distribution of the detected residue is displayed in fig. 7-b. It is shown as a function of the ring number of the experimental setup [21] (2°-3°, 3°-4.5°, 4.5°-7°, and so on ...). In fig. 7-c and 7-d, for QP residues, are plotted the velocity component parallel to the beam axis and the charge distribution. In figs. 7-e and 7-f are shown the experimental multiplicity and energy distributions of the emitted α particles as dashed lines and superimposed as solid lines the gaussian and maxwellian distributions we used as mimics to the experimental distributions, respectively. The even values appearing in fig. 7-e originate from the method used in the reconstruction of QP's (cf. subsect. 3.2.1). The mimic distributions in figs. 7-e and 7-f do not perfectly fit the data, in particular α particles with very low energies are not taken into account. In the same way, the calculated distributions (solid lines in figs. 7-c and 7-d) underestimate the experimental tails at low velocities and small charges, respectively. However these discrepancies only little affect the final results on the value of the angular momentum. Indeed these discrepancies may change the value of the σ width parameter but this effect is small compared to the uncertainties on the average values of the mass and temperature of the emitter. In fig. 6-a is shown the $V_\perp - V_\parallel$ simulated correlation for α particles. It compares well with the data at least in the forward hemisphere of QP's.

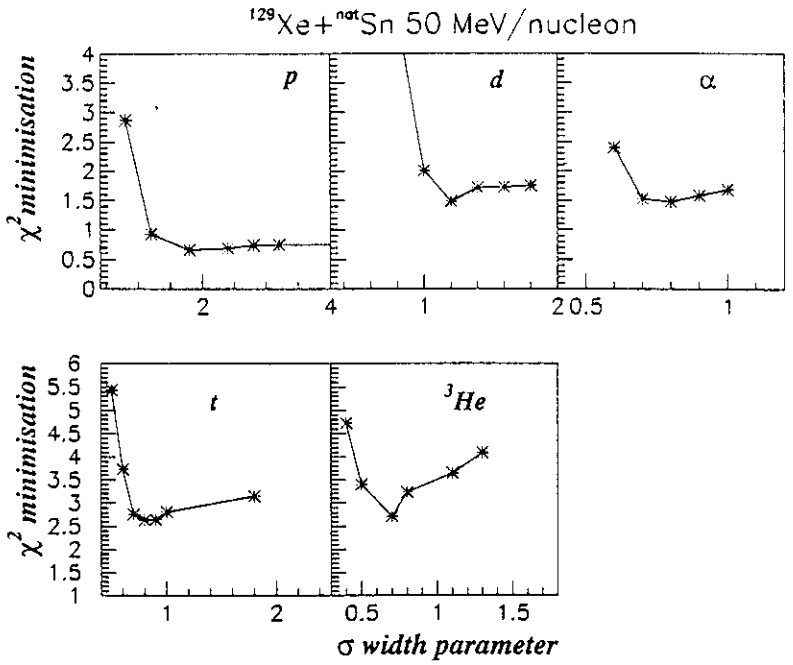

Fig. 8. Evolution of the χ^2 parameter as a function of the σ width parameter of the angular distribution of LCP's associated to events with $50 < E_\perp \leq 100$ MeV (see text).

As explained above once the distributions of the residue are reproduced, the corresponding initial distributions of the QP are saved and used in new calculations of the angular distributions of LCP's in which the σ parameter (eq. (7)) is changed step by step. The best solution is obtained by a minimization procedure as illustrated in fig. 8. In this figure is plotted the value of the $\chi^2 = \sum_i (W_i^{exp} - W_i^{cal})^2$ parameter as a function of the value of the σ parameter. These results concern LCP's emitted by QP's produced in peripheral collisions with $50 < E_\perp \leq 100$ MeV. The asymmetrical shape of the correlation is observed with all LCP's. Keeping in mind that the spin value is inversely proportional to the σ parameter, this asymmetrical behaviour reflects a higher sensitivity of the angular distributions to the high spin values than to the low ones.

In fig. 5 are displayed the simulated and experimental angular distributions of α particles emitted by QP's produced in collisions with $50 < E_\perp \leq 100$ MeV. As can be seen the experimental flat distributions (full histograms in fig. 5) observed at positive in-plane angles are now quite well reproduced by the calculations (dashed histograms in fig. 5). From the comparaison between data and calculations, we extract a value for the width of the angular distributions of $\sigma = 0.85$. With a temperature of 4.8 MeV (cf. table 1) and an average atomic mass of 109 for the residual nucleus, a spin value of $(43 \pm 13)\ \hbar$ is deduced, the uncertainty being mainly due to the uncertainties on the average mass of the emitter and on its temperature.

In fig. 9 are displayed the angular distributions of α particles emitted in collisions with $150 < E_\perp \leq 200$ MeV. The angular distributions are nicely reproduced at positive in-

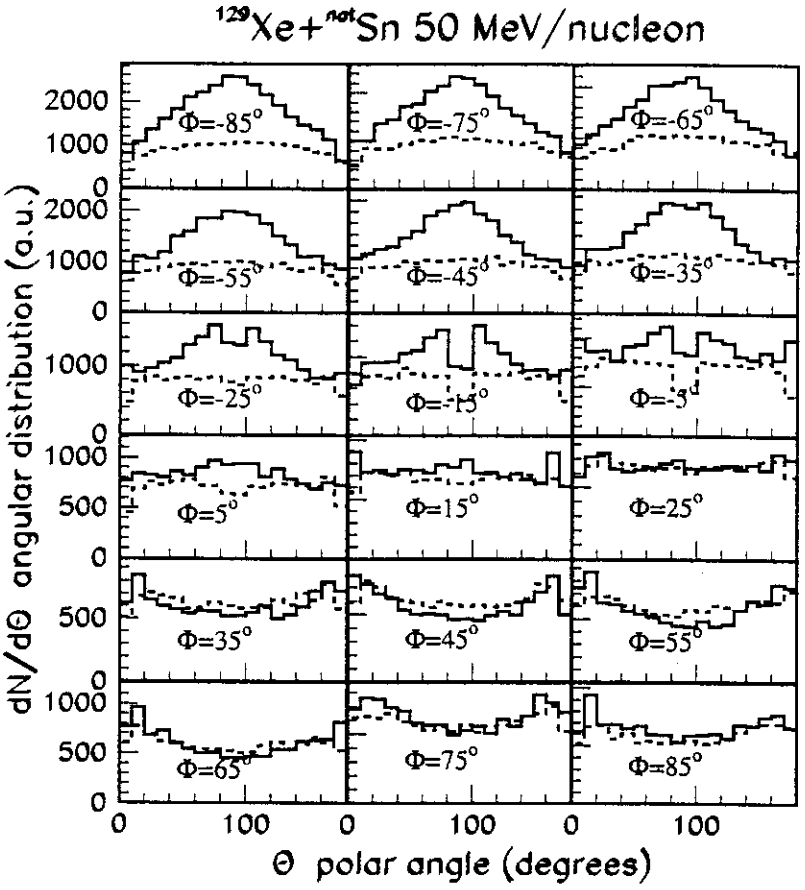

Fig. 9. Out-of-plane angular distributions shown as a function of the in-plane angle. These data concern α particles emitted from QP's produced in events with $150 < E_{\perp} \leq 200$ MeV. Solid lines are the data, dashed lines are results of a simulation (see text).

plane angles, when the particles are emitted on the same side of the beam as the residue. Nevertheless the yield of particles observed at negative in-plane angles is not accounted for. When looking at the experimental data in the velocity plane an excess of particles rises in the backward hemisphere in the QP frame (cf. fig. 6-b). This yield is attributed to the mid-velocity component, it increases with the increase of the dissipation. For the more dissipative collisions a contamination of these mid-velocity particles in the forward hemisphere in the QP frame cannot be excluded. As the non statistical particles populate mainly the negative in-plane angles, only experimental data measured at positive in-plane angles have been kept in the analysis. Only for the specific bin $150 < E_{\perp} \leq 200$ MeV the σ parameter was obtained by fitting the angular distribution in the angular range $0° < \Phi < 90°$. This is the reason why the experimental data (full histograms in fig. 9) are reproduced by the calculations (dashed histograms in fig. 9) in the limited range of positive in-plane angles. From this figure, it can be noted how intimately mixed are the statistically and non statistically emitted particles and how difficult it appears to disentangle the two contributions.

8 Spin values of QP's extracted from the angular distributions of LCP's

The simulation has been performed for all types of LCP's (p, d, t, ^{3}He and α) and for several bins in $E_\perp$. As already mentioned, $E_\perp$ is used here as a rough impact parameter selector. All results are shown in fig. 10.

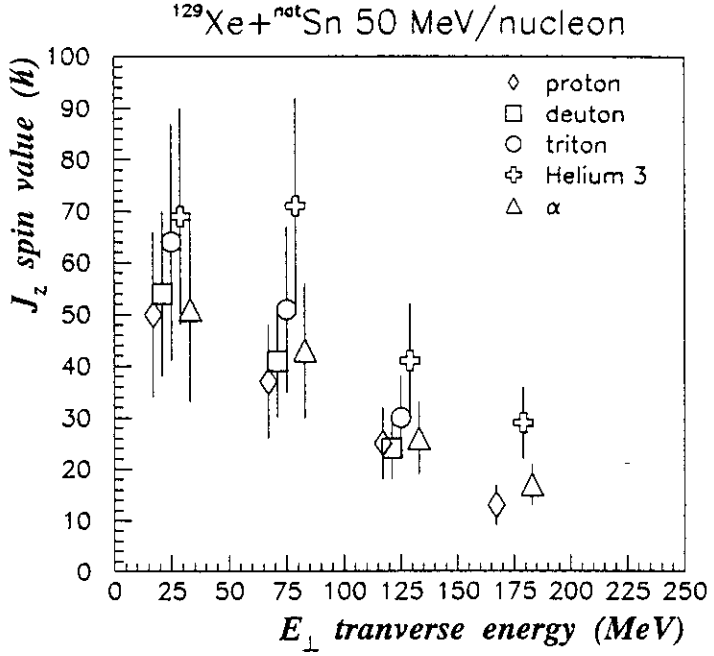

Fig. 10. Apparent spin values of QP's deduced from the angular distributions of p, d, t, ^{3}He and α as a function of the transverse energy. For clarity, symbols have been shifted along the abscissa axis. Uncertainties on the spin determination are shown as error bars.

The striking feature coming out from fig. 10 is the decrease of the spin value with the increase of the transverse energy, whatever the nature of LCP's. Such a behaviour has already been observed in fig. 4. In peripheral reactions the angular momentum transfer is expected to originate from the coupling of the relative motion of the target and projectile and of the internal motion of nucleons in the target and projectile [57]. The angular momentum associated with the conversion of the orbital motion into intrinsic rotation is aligned along the normal to the reaction plane while the angular momentum associated with the Fermi motion of the transferred nucleons is randomly distributed in a plane perpendicular to the axis joining the target and projectile. With the increase of the dissipation more nucleons are transferred into the two nuclei: the component associated with the orbital motion growing more that the component associated with the Fermi motion (due to the random nature of this mechanism) [57]. As a result the magnitude of the angular momentum transfer is expected to increase with the dissipation. As seen in fig. 10 the trend of the experimental data is at variance with this expectation.

This picture does not hold any longer for highly dissipative collisions. Indeed, nucleons

are no more exchanged on the periphery of the nuclei and through a small window. As a consequence individual transfers from relative orbital motion are smaller in magnitude and no more aligned along the normal to the reaction plane, leading to a much smaller component.

Actually, the spin values extracted from the angular distributions of LCP's correspond to values averaged over the whole deexcitation chain undergone by QP's. In that sense these values are apparent spin values in the same way as the slope parameter of a kinetic energy spectrum represents only an apparent temperature. As a consequence, the values plotted in fig. 10 do not reflect the initial spin values of QP's and cannot be directly compared with predictions of theoretical models.

Spin values displayed in figs. 4 and 10 exhibit the same behaviour. However in fig. 4, spin values are systematically higher than those plotted in fig. 10, the discrepancy increasing with $E_\perp$. In fig. 4, the spin values are deduced from the kinetic energy of LCP's integrated over the angular range $-90° \leq \Phi \leq 90°$. With the increase of $E_\perp$, the mid-velocity particles populate more and more the forward hemisphere of the QP frame as seen in sects. 6 and 7. As these particles are preferentially emitted in the reaction plane and have larger transverse energies [39], they contribute to increase the mean kinetic energy measured in the plane, compared to the mean kinetic energy measured out-of-plane. The consequence is a higher $\Delta < E >$ value and therefore a higher spin value (see eq. (8)). Note that the dispersion of the spin values is less in fig. 4 than in fig. 10. It is attributed to the fact that values extracted from kinetic energies (fig. 4) do not depend on the temperature of the emitter.

9 Angular momentum transfer as a function of Z_{max} and E_{bomb}

AMT has been analysed as a function of the atomic number Z_{max} of the detected QP residue and as a function of the bombarding energy E_{bomb} for events associated with $E_\perp < 75$ MeV at 25 MeV/nucleon, 117 MeV at 39 MeV/nucleon and 150 MeV at 50 MeV/nucleon. Only protons and α particles have been looked for, the statistics being too low for the other LCP's. The spin is extracted from the out-of-plane angular distributions integrated over the forward hemisphere of the QP (in-plane angles between -90° and 90°). It has been checked with the simulation that deriving the spin from the whole $W(\Theta,\Phi)$ angular distribution or from the Φ integrated $W(\Theta)$ distribution does not change significantly the results. The spin values obtained from the angular distributions of α-particles and protons are shown in figs. 11-a and -b, respectively, and for different bombarding energies: 25 (squares), 39 (triangles) and 50 (filled circles) MeV/nucleon.

The angular momentum decreases slightly with the decrease of the atomic number of the detected QP, whatever the bombarding energy and the particle. Measurements done at 50 and 39 MeV/nucleon are very close from each other while larger values are observed at the lowest bombarding energy of 25 MeV/nucleon.

Spin values extracted from protons (fig. 11-b) are slightly higher than spin values extracted from α-particles (fig. 11-a). This behaviour agrees with statistical model calculations, as Gemini [58], in which proton emission is associated to a mean spin value which is, on average,

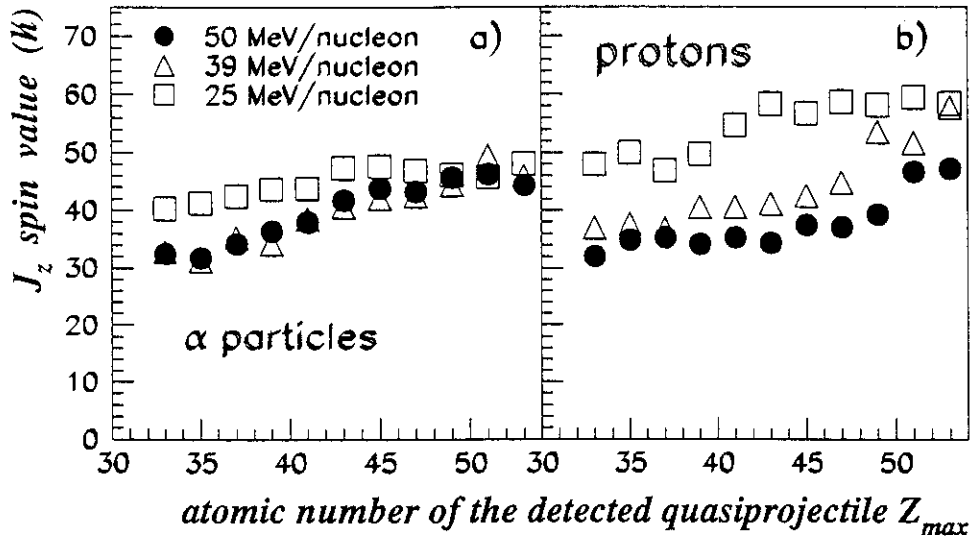

Fig. 11. Spin value of QP's produced in the collisions ^{129}Xe+^{nat}Sn at different bombarding energies. The spin values are extracted from the angular distributions of α-particles (a) and protons (b).

higher than the spin value for α-emission, the highest spin value being associated with deuterons and tritons.

It should be noted that the experimental values obtained for QP's with atomic number very close to that of the projectile are higher than they should be, due to a wrong reconstruction of the reaction plane, which leads to a strong anisotropy of the angular distribution and consequently to a high spin value of QP's. So the right behaviour of the data displayed in figs. 11-a and -b should be, for QP's close to the projectile, a decrease of the spin value when the atomic number increases.

10 Results and discussion

10.1 Apparent spins and temperatures

For the ^{129}Xe+^{nat}Sn collisions at 50 MeV/nucleon, are given in table 1 the slope parameters (apparent temperatures) of the kinetic energy spectra of LCP's measured along the spin axis in order to minimize any influence of the angular momentum. The higher apparent temperatures are clearly associated to ^{3}He nuclei, similar values are obtained for deuterons, tritons and α particles while protons have always the smallest values.

From the data shown in fig. 10 it appears that ^{3}He (and to a lesser extent ^{3}H) are linked to higher spin values than the other particles, those particles (p, d and α) leading to approximately the same values. From eq. (7) it is obvious that high spin values are connected to high temperature values. Significantly larger spins are still deduced for ^{3}He if the same

temperature is fixed for all LCP's in eq. (7). No such effect appears when looking at spin values deduced from kinetic energies (see fig. 4). Recall that these values are independent of the temperature of the emitter.

$E_\perp$ (MeV)	0-50	50-100	100-150	150-200
p	3.2	3.8	4.1	4.7
d	4.4	4.9	5.2	6.2
t	3.7	4.3	5.3	6.1
^{3}He	5.8	6.5	8.	8.6
α	3.8	4.8	5.7	6.1

Table 1
Slope parameters in MeV of the kinetic energy spectra of LCP's as a function of the $E_\perp$ transverse energy, measured in the ^{129}Xe+^{nat}Sn collisions at 50 MeV/nucleon.

As for the other particles it is hard to see any hierarchy in the emission time looking both at the apparent spin and temperature values. It seems that these particles are emitted at any time.

10.2 Comparison of the data with predictions of dynamical models

In the nucleon exchange transport (NET) model of Randrup [11] the energy and angular momentum are dissipated in the relative motion via the stochastic exchange of nucleons between the two partners during the interaction. In this model usual dynamical variables are taken into account as well as the three spin components of each nucleus which are explicitely introduced. No deexcitation step is included in the calculation, so in order to compare with the data, we assume that every evaporated nucleon carries away 12 MeV of excitation energy [48].

The Simon code of Durand [53], uses the same formalism to describe dynamically the interaction between the two ions. The statistical deexcitation of the nuclei is performed in a standard way with a time dependence for the emission of particles and fragments.

AMT has also been studied with the help of the semi-classical Landau-Vlasov model (LV) [15,59]. Some results have been obtained from these dynamical calculations using the finite range Gogny interaction [15]. Calculations have been done as a function of the impact parameter. The conversion in a $E_\perp$ scale or in a scale of the atomic number of the largest fragment is based on experimental works [34,48].

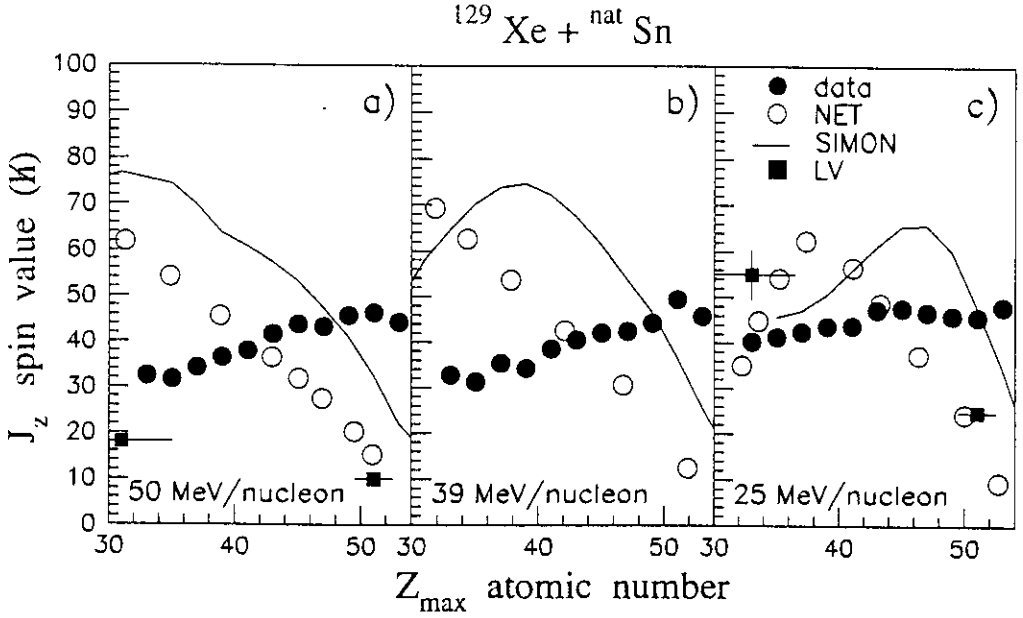

Fig. 12. -a) Theoretical predictions of the spin value from the NET model [11] (open circles), the Landau-Vlasov model [15] (filled squares) and the Simon model [53] (lines) are compared to the data (filled circles) at 50 MeV/nucleon (-a), 39 MeV/nucleon (-b) and 25 MeV/nucleon (-c).

10.2.1 Spin values as a function of Z_{max} and E_{bomb}

The spin values extracted from the data are compared to model predictions in fig. 12 at three bombarding energies. All calculated values correspond to the initial spin value of QP's while the data are apparent values. In that comparison calculations have not been filtered by the experimental setup.

At 25 MeV/nucleon, the NET and LV calculations agree between them. The predictions of the Simon model, while exhibiting the same behaviour, are shifted along the atomic number axis due to an energy dissipation found smaller in this model than in the two other ones. As already mentioned in sect. 9, the experimental spin values of QP's very close to the projectile are overestimated. So the discrepancy with the calculations is obvious for the limited range Z > 45-50. For atomic numbers below 45-50, a qualitative agreement is seen at 25 MeV/nucleon (fig. 12-c), taking into account that data are only apparent values and therefore smaller than initial spin values.

With the increase of the bombarding energy the disagreement between data and calculations becomes larger. It is seen at 39 MeV/nucleon (fig. 12-b) when comparing the data to the predictions of the NET and Simon models. It is even worse at 50 MeV/nucleon (fig. 12-a) where predicted spin values increase continuously up to 60-80 $\hbar$ with the decrease of the atomic number. At these bombarding energies, the mechanisms of AMT, as known from the low energy studies such as nucleon transfers, are likely less effective: either these particles waste a fraction of the initial spin leaving less spin to be transferred to the reaction partners, or possibly the reaction mechanisms at intermediate bombarding energy (n-n collisions?) do not transfer as much spin as the one-body dissipation does at lower energy.

When looking at the LV calculations at 50 MeV/nucleon, a better agreement can be seen with the data although calculated values are smaller. With the increase of the bombarding energy, the LV calculations lead to a smaller spin value as indicated by these experimental data and other observations [15,27]. This behaviour, not reproduced by the NET and Simon transport models, is attributed to the increasing role of the two-body interactions as and when the incident energy goes up.

10.2.2 Spin values as a function of $E_\perp$

In fig. 13 are displayed data already shown in fig. 10 together with the predictions of the Simon code [53]. These results concern the ^{129}Xe+^{nat}Sn collisions at 50 MeV/nucleon. Filled circles represent the initial spin value of QP's as a function of the transverse energy. As expected the spin value increases with the increase of the transverse energy. A meaningful comparison between data and model needs that simulated events be filtered by the experimental setup and analysed with the same procedure as the experimental data. This has been done for α particles (empty circles in fig. 13). An excellent agreement is seen for peripheral collisions with $E_\perp \leq 100$ MeV. Above the discrepancy increases with the increase of the transverse energy. As we know the contribution of mid-velocity particles start to develop and AMT may become less effective.

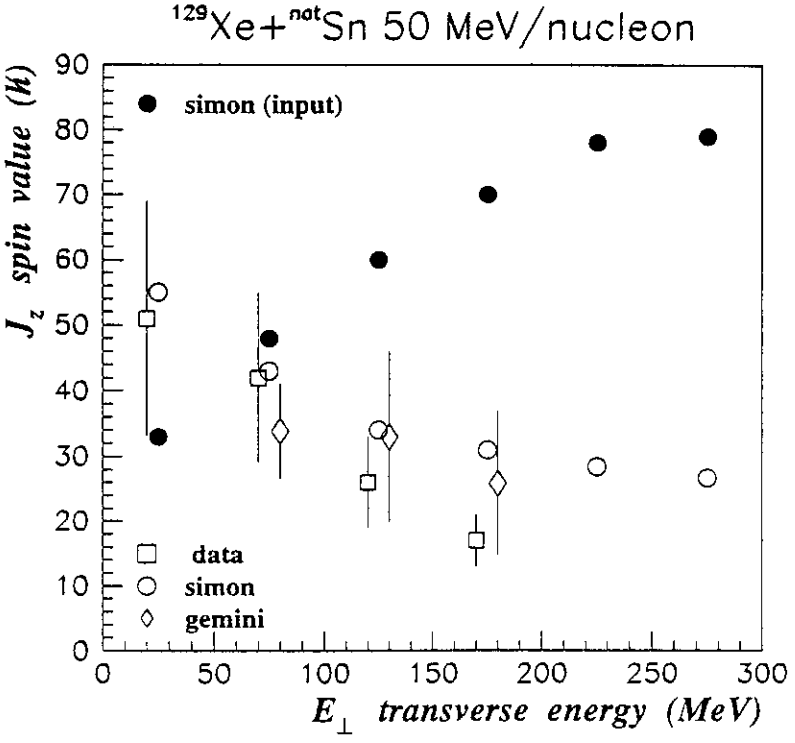

Fig. 13. Apparent spin values extracted from the angular distributions of α particles. The data (open squares) are compared with the model predictions of refs. [53] (empty circles) and [58] (diamonds). The filled circles represent the initial spin value of QP's [53]. Uncertainties on the spin values are shown as error bars.

As already noticed at the end of sect. 9, the less dissipative collisions suffer from a bad

reconstruction resulting in higher spin values than they should be: at $< E_\perp >= 25$ MeV the spin value deduced from the filtered calculations is found larger than the input value (empty circle compared to filled one in fig. 13). However experimental data and filtered calculations agree very well (open square and empty circle in fig. 13).

10.3 Comparison of the data with predictions of a statistical model

Calculations have also been performed with the statistical code Gemini [58] for QP's with given values of excitation energy and angular momentum. The excitation energies of 1.0, 2.0 and 3.0 MeV/nucleon have been chosen as they roughly correspond to the mean excitation energy of QP's produced in collisions associated with a mean transverse energy of 75, 125 and 175 MeV, respectively. These values are slightly lower than those displayed in fig. 1-c as the latter values deal with "complete events" (both QP and QT are detected in violent collisions) while the former ones concern events associated with a detection of more than 70% of the incident momentum. As for the spin, values of 50, 60 and 70 $\hbar$ have been retained to match approximately the initial spin value predicted by the Simon code. Calculations have been performed using the options available in the Gemini code concerning the IMF's emission: (opt. 0) only the evaporation of LCP's from the compound nucleus is accounted for, (opt. 1) symmetric fission of the compound nucleus and evaporation of LCP's are considered and (opt. 2) all divisions are taken into account (the symmetric ones as well as the asymmetric ones).

First it should be noted that options 0 and 1 give similar results. The multiplicities of evaporated LCP's (n, p, d, t, α) are very close from each other in the two calculations. Only small deviations are observed with the increase of the spin value, the largest difference being seen for α particles. Indeed a multiplicity of 2.09 is obtained using option 0 while a multiplicity of 1.77 is obtained with option 1: the emission of α particles is favored in case of high spins (i-e when there is no fission of the compound nucleus) than in case of low spins (the fission of the compound nucleus leaves two fragments with low spins). Such an observation is well understood for Xe-like nuclei which exhibit a high barrier against fission.

When considering option 2 it turns out that the calculated number of IMF's is larger than the experimental one. The yield of IMF's is overestimated. However, averaging the calculations of options 0 and 2 (or 1 and 2, it is equivalent) leads to values in rough agreement with the data as it is shown in table 2. Once it has been checked that the predictions of the Gemini code are in reasonable agreement with the data, at least concerning the multiplicities of LCP's emitted by QP's, the predictions on AMT can be looked at. For that comparison, the angular distributions of LCP's have not been built in the QP frame as done in subsect. 10.2.2. Instead for given E^* and J values input in Gemini the mean spin value is the mean value of the spin distribution of all daughter nuclei having emitted α particles for a given $E_\perp$ bin. The mean value of QP's spin distribution associated with α-emission is displayed in fig. 13 (diamonds). The error bars reflect the standard deviation of the calculated distributions. A satisfactory agreement can be stated from the comparison of the data with the calculations. In particular the observed decrease of the spin value with the increase of the E^* (and then of $E_\perp$) is correctly reproduced, although large uncertainties are associated with both of them.

particle	$M_{exp.}$	$M_{calc.}$	$M_{exp.}$	$M_{calc.}$	$M_{exp.}$	$M_{calc.}$
p	.78±.09	.25±.02	1.64±.08	1.31±.04	2.09±.08	2.31±.04
d	.18±.03	.04±.01	.39±.05	.38±.02	.60±.04	.83±.03
t	.09±.03	.02±.01	.13±.03	.18±.01	.28±.03	.40±.02
α	.55±.07	.57±.03	1.04±.07	1.16±.04	1.58±.09	1.47±.04
$3 < Z \leq 8$	.08±.03	.12±.01	.25±.03	.47±.02	.42±.04	.74±.02

Table 2
Experimental particle multiplicities and particle multiplicities calculated with the Gemini code [58]. Rows 2 and 3 correspond to QP's produced in the ^{129}Xe+^{nat}Sn collisions at 50 MeV/nucleon with a transverse energy $< E_\perp >$ of 75 MeV, rows 4 and 5 to $< E_\perp > = 125$ MeV and rows 6 and 7 to $< E_\perp > = 175$ MeV (see text).

It should be noted here that the multiplicity ratio $< M_p > / < M_\alpha >$ deduced from the data are in excellent agreement with those inferred from the recent work of ref. [61] performed on the direct and reverse collisions of ^{93}Nb and ^{116}Sn at 25 MeV/nucleon.

11 Conclusions

In this work we studied the properties of QP's produced in the ^{129}Xe+^{nat}Sn collisions at intermediate bombarding energies. The excitation energy per nucleon has been derived from the experimental data using several prescriptions. Whatever the prescription, the excitation increases linearly with the violence of the collision and then saturates. In the most violent collisions, at 50 MeV/nucleon, the excitation energy may reach $\approx$ 10 MeV/nucleon.

The amount of angular momentum imparted to QP's has also been studied. The spin values have been extracted from both the kinetic energy spectra and angular distributions of LCP's (p, d, t, ^{3}He and α). Both methods agree qualitatively. In particular, the spin determination from the mean value of the kinetic energy spectra of LCP's appear to be powerful due to its simplicity and due to the fact that it does not require any assumption on the temperature of the emitter.

The spin value is seen to decrease as a function of the violence of the collision (measured from the transverse energy or the detected QP charge) . It has been demonstrated that this behaviour is linked to the deexcitation chain of QP's. Theoretical calculations, dynamical as well as statistical, reproduce the experimental behaviour. Transport model calculations filtered by the experimental setup and analysed in the same way as the data describe nicely the low dissipation energy. A discrepancy grows up with the energy dissipation which could be explained by the role of mid-velocity particles. This statement is reinforced by the fact that higher spin values are measured at 25 MeV/nucleon than at 39 and 50 MeV/nucleon,

as predicted by semi-classical calculations.

Building the angular distributions of LCP's (or fission fragments) to determine AMT is a neat procedure. At low dissipation this technique is particularly powerful while the multiplicity of LCP's is weak. In that case the spin value deduced from the angular distributions, especially for fission events, reflects the initial spin value of the nuclei. At higher dissipation, the use of this method is questionable. On one hand it becomes more and more difficult selecting LCP's emitted by the nuclei. On the other hand their high multiplicity leads to an average over the deexcitation chain, the spin value being only an apparent value associated with a rather large uncertainty due to the assumptions made on the mass and temperature of the emitter.

This work shows the limits of such an analysis. Further improvements can only be accessed through comparisons between raw data and predictions of theoretical models aiming at reproducing as accurately as possible all experimental observables, in particular the mid-velocity component which might be a major contribution in the dissipative phenomena at intermediate incident energies [62–64].

Such sophisticated calculations are needed, for example, to provide insight on the dealignment mechanism of AMT [10,11,16,17]. In principle from the total angular distribution it should be possible to deduce the magnitude of each spin component: it requests that equilibrium particles emitted from QP's be disentangled from those coming from non equilibrium processes. Such a determination was not feasible in this analysis.

The one-body dissipation still applies at intermediate energies and for collisions with moderate energy dissipation. Large spin values (50-60 $\hbar$) are transferred to QP's. However, for higher energy dissipations, LCP's and IMF's emitted early in the interaction may take away a fraction of the initial orbital angular momentum leaving less angular momentum to be transferred to the nuclei, or may dissipate a fraction of the intrinsic spins of these nuclei. The role of the two-body dissipation and its influence on AMT has to be investigated more in these collisions. Semi-classical calculations including two-body interactions seem to account for that effect.

References

[1] W.U. Schröder and J.R. Huizenga, in Treatise on Heavy-Ion Science, edited by D.A. Bromley (Plenum, New-York, 1984), vol. 2.

[2] L.G. Moretto and G.J. Wozniak, Annu. Rev. Nucl. Part. Sci. **43** (1993) 379.

[3] J.B. Natowitz, M.N. Namboodiri, P. Kasiraj, R. Eggers, L. Adler, P. Gonthier, C. Cerruti and T. Alleman, Phys. Rev. Lett. **40** (1978) 751.

[4] R.A. Dayras, R.G. Stokstad, D.C. Hensley, M.L. Halbert, D.G. Sarantites, L. Westerberg and J.H. Barker, Phys. Rev. **C22** (1980) 1485.

[5] R. Babinet, B. Cauvin, J. Girard, J.M. Alexander, T.H. Chiang, J. Galin, B. Gatty, D. Guerreau and X. Tarrago, Z. Phys. **A295** (1980) 153.

[6] P. Dyer, R.J. Puigh, R. Vandenbosch, T.D. Thomas and M.S. Zisman, Phys. Rev. Lett. **39** (1977) 392.

[7] D. von Harrach, P. Glässel, Y. Civelekoglu, R. Männer and H.J. Specht, Phys. Rev. Lett. **42** (1979) 1728.

[8] J.C. Steckmeyer, F. Lefebvres, C. Le Brun, J.F. Lecolley, M. L'Haridon, A. Osmont and J.P.Patry, Nucl. Phys. **A427** (1984) 357.

[9] M. Lefort and C. Ngô, Ann. de Phys. **3** (1978) 5.

[10] L.G. Moretto and R.P. Schmitt, Phys. Rev. **C21** (1980) 204.

[11] J. Randrup, Nucl. Phys. **A383** (1983) 468.

[12] W. Trautmann *et al.*, in Proceedings of the XXXIst International Winter Meeting on Nuclear Physics, Bormio, Italy, ed. I. Iori (Univ. di Milano, Milano, 1993).

[13] M.N. Namboodiri, R.K. Choudhury, L. Adler, J.D. Bronson, D. Fabris, U. Garg, P.L. Gonthier, K. Hagel, D.R. Haenni, Y.W. Lui, Z. Majka, G. Mouchaty, T. Murakami, J. B. Natowitz, G. Nebbia, R. P. Schmitt, S. Simon, J. P. Sullivan and D.H. Youngblood, Phys. Rev. **C35** (1987) 149.

[14] J. Colin, G. Bizard, D. Durand, A. Genoux-Lubain, C. Le Brun, J.F. Lecolley, M. Louvel, Ch. Meslin, G. Rudolf, J.C. Steckmeyer and L. Stuttgé, Nucl. Phys. **A593** (1995) 48 and references therein.

[15] F. Haddad, B. Borderie, V. de la Mota, M.F. Rivet, F. Sébille and B. Jouault, Z. Phys. **A354** (1996) 321.

[16] R.A. Broglia, C.H. Dasso, G. Pollarolo and A. Winther, Phys. Rev. Lett. **41** (1978) 25.

[17] D.P. Min, J. Phys. **C401** (1978) 431.

[18] W. Cassing, Z. Phys. **A327** (1987) 447.

[19] G.F. Bertsch, Z. Phys. **A289** (1978) 103.

[20] A. Botvina and D.H.E. Gross, Nucl. Phys. **A592** (1995) 257.

[21] J. Pouthas, B. Borderie, R. Dayras, E. Plagnol, M.F. Rivet, F. Saint-Laurent, J.C. Steckmeyer, G. Auger, Ch.O. Bacri, S. Barbey, A. Barbier, A. Benkirane, J. Benlliure, B. Berthier, E. Bougamont, P. Bourgault, P. Box, R. Bzyl, B. Cahan, Y. Cassagnou, D. Charlet, J.L. Charvet, A. Chbihi, T. Clerc, N. Copinet, D. Cussol, M. Engrand, J.M. Gautier, Y. Huguet, O. Jouniaux, J.L. Laville, P. Le Botlan, A. Leconte, R. Legrain, P. Lelong, M. Le Guay, L. Martina, C. Mazur, P. Mosrin, L. Olivier, J.P. Passerieux, S. Pierre, B. Piquet, E. Plaige, E.C. Pollacco, B. Raine, A. Richard, J. Ropert, C. Spitaels, L. Stab, D. Sznajderman, L. Tassan-Got, J. Tillier, M. Tripon, P. Vallerand, C. Volant, P. Volkov, J.P. Wieleczko and G. Wittwer, Nucl. Instr. and Meth. **A357** (1995) 418.

[22] J.C. Steckmeyer, D. Cussol, J. Duchon, J.M. Gautier, J.L. Laville, P. Le Botlan, A. Leconte, J. Lelandais, V. Métivier, P. Mosrin, E. Rosato, J. Tillier and A. Wieloch, Nucl. Instr. and Meth. **A361** (1996) 472.

[23] R. Dayras, R. Coniglione, J. Barette, B. Berthier, D.M. de Castro Rizzo, O. Cisse, F. Gadi, R. Legrain, M.C. Mermaz, H. Delagrange, W. Mittig, B. Heusch, G. Lanzanó and A. Pagano, Phys. Rev. Lett. **62** (1989) 1017.

[24] J. Péter, S.C. Jeong, J.C. Angélique, G. Auger, G. Bizard, R. Brou, A. Buta, C. Cabot, Y. Cassagnou, E. Crema, D. Cussol, D. Durand, Y. El Masri, P. Eudes, Z.Y. He, A. Kerambrun, C. Lebrun, R. Legrain, J.P. Patry, A. Péghaire, R. Régimbart, E. Rosato, F. Saint-Laurent, J.C. Steckmeyer, B. Tamain and E. Vient, Nucl. Phys. **A593** (1995) 95.

[25] Y. Larochelle, C. St-Pierre, L. Beaulieu, N. Colonna, L. Gingras, G.C. Ball, D.R. Bowman, M. Colonna, G. D'Erasmo, E. Fiore, D. Fox, A. Galindo-Uribarri, E. Hagberg, D. Horn, R. Laforest, A. Pantaleo, R. Roy and G. Tagliente, Phys. Lett. **B352** (1995) 8.

[26] J.C. Steckmeyer, A. Kerambrun, J.C. Angélique, G. Auger, G. Bizard, R. Brou, C. Cabot, E. Crema, D. Cussol, D. Durand, Y. El Masri, P. Eudes, M. Gonin, K. Hagel, Z.Y. He, S.C. Jeong, C. Lebrun, J.P. Patry, A. Péghaire, J. Péter, R. Régimbart, E. Rosato, F. Saint-Laurent, B. Tamain, E. Vient and R. Wada, Phys. Rev. Lett. **76** (1996) 4895.

[27] D. Jouan, B. Borderie, M.F. Rivet, C. Cabot, H. Fuchs, H. Gauvin, C. Grégoire, F. Hanappe, D. Gardès, M. Montoya, B. Remaud and F. Sébille, Z. Phys. **A340** (1991) 63.

[28] J.E. Sauvestre, J.L. Charvet, R. Dayras, C. Volant, B. Berthier, R. Legrain, R. Lucas, E.C. Pollacco, E. De Filippo, G. Lanzanó, A. Pagano, C. Beck and B. Djerroud, Phys. Lett. **B335** (1994) 300.

[29] B. Lott, S.P. Baldwin, B.M. Szabo, B.M. Quednau, W.U. Schröder, J. Töke, L.G. Sobotka, J. Barreto, R.J. Charity, L. Gallamore, D.G. Sarantites, D.W. Stracener and R.T. De Souza, Phys. Rev. Lett. **68** (1992) 3141.

[30] J.F. Lecolley, L. Stuttgé, M. Aboufirassi, B. Bilwes, R. Bougault, R. Brou, F. Cosmo, J. Colin, D. Durand, J. Galin, A. Genoux-Lubain, D. Guerreau, D. Horn, D. Jacquet, J.L. Laville, F. Lefebvres, C. Le Brun, O. Lopez, M. Louvel, M. Mahi, C. Meslin, M. Morjean, A. Péghaire, G. Rudolf, F. Scheibling, J.C. Steckmeyer, B. Tamain and S. Tomasevic, Phys. Lett. **B325** (1994) 317.

[31] A. Stefanini, G. Casini, P.R. Maurenzig, A. Olmi, R.J. Charity, R. Freifelder, A. Gobbi, N. Herrmann, K.D. Hildenbrand, M. Petrovici, F. Rami, H. Stelzer, J.P. Wessels, M. Gnirs, D. Pelte, J. Galin, D. Guerreau, U. Jahnke, A. Péghaire, J.C. Adloff, B. Bilwes, R. Bilwes and G. Rudolf, Z. Phys. **A351** (1995) 167.

[32] V. Métivier, Thesis, Caen, 1995

[33] J. Łukasik, J. Benlliure, V. Métivier, E. Plagnol, B. Tamain, M. Assenard, G. Auger, Ch.O. Bacri, E. Bisquer, B. Borderie, R. Bougault, R. Brou, Ph. Buchet, J.L. Charvet, A. Chbihi, J. Colin, D. Cussol, R. Dayras, A. Demeyer, D. Doré, D. Durand, E. Gerlic, M. Germain, D. Gourio, D. Guinet, P. Lautesse, J.L. Laville, J.F. Lecolley, A. Le Fèvre, T. Lefort, R. Legrain, O. Lopez, M. Louvel, N. Marie, L. Nalpas, M. Parlog, J. Péter, G. Politi, A. Rahmani, T. Reposeur, M.F. Rivet, E. Rosato, F. Saint-Laurent, M. Squalli, J.C. Steckmeyer, M. Stern, L. Tassan-Got, E. Vient, C. Volant, J.P. Wieleczko, M. Colonna, F. Haddad, Ph. Eudes, T. Sami and F. Sébille, Phys. Rev. **C55** (1997) 1906.

[34] E. Plagnol, J. Łukasik, G. Auger, Ch.O. Bacri, N. Bellaize, F. Bocage, B. Borderie, R. Bougault, R. Brou, P. Buchet, J.L. Charvet, A. Chbihi, J. Colin, D. Cussol, R. Dayras, A. Demeyer, D. Doré, D. Durand, J.D. Frankland, E. Galichet, E. Genouin-Duhamel, E. Gerlic, D. Guinet, P. Lautesse, J.L. Laville, J.F. Lecolley, R. Legrain, N. Le Neindre, O. Lopez, M. Louvel, A.M. Maskay, L. Nalpas, A.D. N'Guyen, M. Pârlog, J. Péter, M.F. Rivet, E. Rosato, F. Saint-Laurent, S. Salou, J.C. Steckmeyer, M. Stern, G. Tăbăcaru, B. Tamain, L. Tassan-Got, O. Tirel, E. Vient, C. Volant and J.P. Wieleczko, Phys. Rev. **C61** (1999) 014606.

[35] V. Métivier, B. Tamain, G. Auger, Ch.O. Bacri, J. Benlliure, F. Bocage, B. Borderie, R. Bougault, R. Brou, Ph. Buchet, J.L. Charvet, A. Chbihi, J. Colin, D. Cussol, R. Dayras, A. Demeyer, D. Doré, D. Durand, P. Ecomard, P. Eudes, D. Gourio, D. Guinet, R. Laforest, P. Lautesse, J.L. Laville, L. Lebreton, J.F. Lecolley, A. Le Fèvre, R. Legrain, O. Lopez, M. Louvel, N. Marie, L. Nalpas, M. Parlog, J. Péter, E. Plagnol, A. Rahmani, T. Reposeur, M.F. Rivet, E. Rosato, F. Saint-Laurent, J.C. Steckmeyer, L. Tassan-Got, E. Vient, C. Volant and J.P. Wieleczko, Nucl. Phys. **A672** (2000) 357.

[36] E. Gadioli and P.E. Hodgson, Pre-Equilibrium Nuclear Reactions, Oxford Studies in Nuclear Physics, (Clarendon Press, Oxford, 1992) vol. 2.

[37] L. Stuttgé, J.C. Adloff, B. Bilwes, R. Bilwes, F. Cosmo, M. Glaser, G. Rudolf, F. Scheibling, R. Bougault, J. Colin, F. Delaunay, A. Genoux-Lubain, D. Horn, C. Le Brun, J.F. Lecolley, M. Louvel, J.C. Steckmeyer and J.L. Ferrero, Nucl. Phys. **A539** (1992) 511.

[38] C.P. Montoya, W.G. Lynch, D.R. Bowman, G.F. Peaslee, N. Carlin, R.T. De Souza, C.K. Gelbke, W.G. Gong, Y.D. Kim, M.A. Lisa, L. Phair, M.B. Tsang, J.B. Webster, C. Williams, N. Colonna, K. Hanold, M.A. McMahan, G.J. Wozniak and L.G. Moretto, Phys. Rev. Lett. **73** (1994) 3070.

[39] T. Lefort, D. Doré, D. Cussol, Y.G. Ma, J. Péter, R. Dayras, M. Assenard, G. Auger, Ch.O. Bacri, F. Bocage, R. Bougault, R. Brou, Ph. Buchet, J.L. Charvet, A. Chbihi, J. Colin, A. Demeyer, D. Durand, P. Eudes, J. Frankland, E. Galichet, E. Genouin-Duhamel, E. Gerlic, M. Germain, D. Gourio, D. Guinet, B. Hurst, P. Lautesse, J.L. Laville, J.F. Lecolley, A. Le Fèvre, R. Legrain, N. Le Neindre, O. Lopez, M. Louvel, A.M. Maskay, L. Nalpas, A.D. N'Guyen, M. Parlog, E. Plagnol, G. Politi, A. Rahmani, T. Reposeur, E. Rosato, F. Saint-Laurent, S. Salou, J.C. Steckmeyer, M. Stern, G. Tabacaru, B. Tamain, L. Tassan-Got, O. Tirel, E. Vient, C. Volant, J.P. Wieleczko and A. Wieloch, Nucl. Phys. **A662** (2000) 397.

[40] J.C. Steckmeyer, G. Bizard, R. Brou, P. Eudes, J.L. Laville, J.B. Natowitz, J.P. Patry, B. Tamain, A. Thiphagne, H. Doubre, A. Péghaire, J. Péter, E. Rosato, J.C. Adloff, A. Kamili, G. Rudolf, F. Scheibling, F. Guilbault, C. Lebrun and F. Hanappe, Nucl. Phys. **A500** (1989) 372.

[41] A. Lleres, A. Giorni, H. Elhage, M.E. Brandan, A.J. Cole, P. Désesquelles, D. Heuer, A. Menchaca-Rocha, J.B. Viano, F. Benrachi, B. Chambon, B. Cheynis, D. Drain and C. Pastor, Phys. Rev. **C48** (1993) 2753.

[42] D. Cussol, G. Bizard, R. Brou, D. Durand, M. Louvel, J.P. Patry, J. Péter, R. Régimbart, J.C. Steckmeyer, J.P. Sullivan, B. Tamain, E. Crema, H. Doubre, K. Hagel, G.M. Jin, A. Péghaire, F. Saint-Laurent, Y. Cassagnou, R. Legrain, C. Lebrun, E. Rosato, R. McGrath, S.C. Jeong, S.M. Lee, Y. Nagashima, T. Nakagawa, M. Ogihara, J. Kasagi and T. Motobayashi, Nucl. Phys. **A561** (1993) 298.

[43] J. Benlliure, Thesis, Caen, 1995.

[44] L. Beaulieu, Y. Larochelle, L. Gingras, G.C. Ball, D.R. Bowman, B. Djerroud, D. Doré, A. Galindo-Uribarri, D. Guinet, E. Hagberg, D. Horn, R. Laforest, P. Lautesse, R. Roy, M. Samri and C. St-Pierre, Phys. Rev. Lett. **77** (1996) 462.

[45] E. Vient, A. Badala, R. Barbera, G. Bizard, R. Bougault, R. Brou, D. Cussol, J. Colin, D. Durand, A. Drouet, J.L. Laville, C. Le Brun, J.F. Lecolley, M. Louvel, J.P. Patry, J. Péter, R. Régimbart, J.C. Steckmeyer, B. Tamain, A. Péghaire, P. Eudes, F. Guilbault, C. Lebrun, E. Rosato and A. Oubahadou, Nucl. Phys. **A571** (1994) 588.

[46] E. Vient *et al.* (Indra Collaboration), in preparation.

[47] M. Gonin, L. Cooke, K. Hagel, Y. Lou, J.B. Natowitz, R.P. Schmitt, S. Shlomo, B. Srivastava, W. Turmel, H. Utsunomiya, R. Wada, G. Nardelli, G. Nebbia, G. Vesti, R. Zanon, B. Fornal, G. Prete, K. Niita, S. Hannuschke, P. Gonthier and B. Wilkins, Phys. Rev. **C42** (1990) 2125.

[48] E. Genouin-Duhamel, Thesis, Caen, 1999.

[49] S. Brandt, Ch. Peyrou, R. Sosnowski and A. Wroblewski, Phys. Lett. **12** (1964) 57.

[50] P. Eudes, Z. Basrak and F. Sébille, Phys. Rev. **C56** (1997) 2003.

[51] D. Doré, Ph. Buchet, J.L. Charvet, R. Dayras, L. Nalpas, D. Cussol, T. Lefort, G. Auger, Ch.O. Bacri, N. Bellaize, F. Bocage, B. Borderie, R. Bougault, R. Brou, A. Chbihi, J. Colin, A. Demeyer, D. Durand, J. Frankland, E. Galichet, E. Genouin-Duhamel, E. Gerlic, D. Guinet, S. Hudan, P. Lautesse, J.L. Laville, J.F. Lecolley, C. Leduc, R. Legrain, N. Le Neindre, O. Lopez, M. Louvel, A.M. Maskay, P. Pawłowski, M. Parlog, J. Péter, E. Plagnol, M.F. Rivet, E. Rosato, F. Saint-Laurent, J.C. Steckmeyer, M. Stern, G. Tabacaru, B. Tamain, L. Tassan-Got, O. Tirel, E. Vient, C. Volant and J.P. Wieleczko, submitted to Phys. Rev. Lett.

[52] N.N. Ajitanand, G. La Rana, R. Lacey, D.J. Moses, L.C. Vaz, G.F. Peaslee, D.M. De Castro Rizzo, M. Kaplan and J.M. Alexander, Phys. Rev. **C34** (1986) 877.

[53] D. Durand, Nucl. Phys. **A541** (1992) 266 and D. Durand *et al.*, in preparation.

[54] X. Qian, L. Beaulieu, X. Bai, Y. Larochelle, B. Djerroud, R. Laforest, L. Gingras, R. Roy, M. Samri, C. St-Pierre, G.C. Ball, D.R. Bowman, E. Hagberg and D. Horn, Phys. Rev. **C59** (1999) 269.

[55] Y. Blumenfeld, Ph. Chomaz, N. Frascaria, J.P. Garron, J.C. Jacmart, J.C. Roynette, D. Ardouin and W. Mittig, Nucl. Phys. **A455** (1986) 357.

[56] Ch.O. Bacri, P. Roussel, V. Borrel, F. Clapier, R. Anne, M. Bernas, Y. Blumenfeld, H. Gauvin, J. Herault, J.C. Jacmart, F. Pougheon, J.L. Sida, C. Stéphan, T. Suomijarvi and L. Tassan-Got, Nucl. Phys. **A555** (1993) 477.

[57] R. Vandenbosch, Phys. Rev. **C20** (1979) 171.

[58] R.J. Charity, M.A. McMahan, G.J. Wozniak, R.J. McDonald, L.G. Moretto, D.G. Sarantites, L.G. Sobotka, G. Guariño, A. Pantaleo, L. Fiore, A. Gobbi and K.D. Hildenbrand, Nucl. Phys. **A483** (1988) 371.

[59] S. Bresson, Thesis, Caen, 1993.

[60] P. Eudes, F. Sébille and M.F. Rivet, private communication.

[61] G. Casini, G. Poggi, S. Calamai, P.R. Maurenzig, A. Olmi, G. Pasquali, A.A. Stefanini, N. Taccetti, J.C. Steckmeyer, R. Laforest and F. Saint-Laurent, Phys. Rev. Lett. **83** (1999) 2537.

[62] R. Nebauer, J. Aichelin, M. Assenard, G. Auger, Ch.O. Bacri, F. Bocage, R. Bougault, R. Brou, P. Buchet, J.L. Charvet, A. Chbihi, J. Colin, D. Cussol, R. Dayas, A. Demeyer, D. Doré, D. Durand, P. Eudes, E. Galichet, E. Genouin-Duhamel, E. Gerlic, M. Germain, D. Gourio, D. Guinet, P. Lautesse, J.L. Laville, T. Lefort, R. Legrain, N. Le Neindre, O. Lopez, M. Louvel, A.M. Maskay, L. Nalpas, A.D. N'Guyen, M. Parlog, J. Péter, A. Rahmani, T. Reposeur, E. Rosato, F. Saint-Laurent, S. Salou, J.C. Steckmeyer, M. Stern, G. Tabacaru, B. Tamain, L. Tassan-Got, O. Tirel, E. Vient, C. Volant and J.P. Wieleczko, Nucl. Phys. **A658** (1999) 67.

[63] Z. Basrak and P. Eudes, Proceedings of the 7^{th} International Conference on Clustering Aspects of Nuclear Structure and Dynamics, June 14-19, 1999, Rab, Island of Rab, Croatia.

[64] R. Wada, K. Hagel, J. Cibor, M. Gonin, Th. Keutgen, M. Murray, J.B. Natowitz, A. Ono, J.C. Steckmeyer, A. Kerambrun, J.C. Angélique, G. Auger, G. Bizard, R. Brou, C. Cabot, E. Crema, D. Cussol, D. Durand, Y. El Masri, P. Eudes, Z.Y. He, S.C. Jeong, C. Lebrun, J.P. Patry, A. Péghaire, J. Péter, R. Régimbart, E. Rosato, F. Saint-Laurent, B. Tamain and E. Vient, submitted to Phys. Rev. **C**.